Nucleation and Crystal Growth in Sheared Granular Sphere Packings

Andreea Panaitescu, K. Anki Reddy, and Arshad Kudrolli
Department of Physics, Clark University, Worcester, Massachusetts 01610, USA
(Received 12 August 2011; published 6 March 2012)

We investigate the nucleation of ordered phases, their symmetries, and distributions in dense frictional hard sphere packings as a function of particle volume fraction ϕ, by imposing cyclic shear and constant applied pressure conditions. We show, with internal imaging, that the nucleating crystallites in the bulk consist of 10–60 spheres with hexagonal close packed (hcp) order and nonspherical shape, that are oriented preferentially along the shear axis. Above $\phi = 0.62 \pm 0.005$, crystallites with face centered cubic (fcc) order are observed with increasing probability, and ordered domains grow rapidly. A polycrystalline phase with domains of fcc and hcp order is observed after hundreds of thousands of shear cycles.

DOI: 10.1103/PhysRevLett.108.108001 PACS numbers: 45.70.Qj, 05.65.+b

The nucleation and growth of crystals from initially disordered packings is fundamental to material science and important to self-assembly of ordered solids from discrete elements. It is well known that thermal frictionless hard sphere systems undergo a glass transition above a volume fraction $\phi_g \sim 0.58$ and crystallization above ϕ_g upon application of shear [1,2]. Experiments with colloidal systems have shown the nucleating crystal to be nonspherical, containing about a hundred particles, with a random hexagonal close packed structure [3].

Here, we consider the development of ordered phases in disordered frictional granular sphere packings. Granular materials are athermal and energy has to be input continuously to rearrange particles. Furthermore, friction forces alter the stability criterion at contact compared with the frictionless case, reducing the number of contacts required for stability from 6 to 4 [4]. Both these facts make it difficult to directly apply what has been learned in frictionless hard sphere systems to granular systems. While simulations have shown that friction can affect packing [5] and increase the volume fraction at which disorder can persist in sheared granular flows to well above those seen in frictionless systems [6], ordered packings have been observed upon application of prolonged periods of shear in granular spheres [7,8]. However, nucleation of ordered phases, their symmetry during nucleation, and evolution upon prolonged shear need to be investigated to gain a deeper understanding of crystallization in granular systems.

We address these issues with experiments using a cyclic shear apparatus which is amenable to three-dimensional visualization with a refractive index matching technique. While this technique has been used recently to examine perturbations to disordered packing [9,10], we perform the experiments over unprecedented long periods to observe development of crystals. It is noteworthy that it is difficult to eliminate the gravitational field in three-dimensional granular packings and implement constant volume conditions. Therefore, we do the experiments under constant pressure conditions to have the simplest prescribed conditions. In spite of the many differences, we find remarkable similarity in the development of order in our experiments on granular spheres when compared with those reported in colloidal systems [3].

A schematic diagram of the shear cell filled with glass beads with a diameter $d = 1.034 \pm 0.03$ mm is shown in the inset in Fig. 1(a). A normal stress of $\sigma_{\mathbf{z}} = -0.4\ \mathbf{k}$ Pa is applied on the top boundary of the cell which is free to move vertically as the packing fraction changes upon application of shear. This stress is an order of magnitude greater than the weight of the grains and is observed to remove the effects of gravitational gradients on the observed packings. A refractive index matched interstitial liquid [11] with a small amount of fluorescent dye is illuminated with a laser light sheet. The particles appear dark in contrast and are imaged with a digital camera from an orthogonal direction. A stack of images is then obtained by linearly translating the plane of illumination along with the camera to measure the position of all particles with a precision of $0.1d$ in three dimensions using standard image processing. The side walls of the cell are slowly tilted between $\pm\pi/36$ rad to quasistatically shear the system and avoid any lubrication effects due to the interstitial liquid. A more detailed description of the apparatus and the imaging technique can be found in Ref. [10].

The volume fraction of the glass beads ϕ in the entire system is obtained by measuring the height of the top surface of the cell as a function of shear cycle N_{sc} applied over a 4 month period [12]. The volume fraction is observed to increase well above the random close packing fraction ϕ_{rcp} of 0.637 [13] over hundreds of thousands of shear cycles. A cross sectional image of the initial random packing and the polycrystalline phase which develops after $N_{\mathrm{sc}} = 5 \times 10^5$ is shown in Fig. 1(b) and 1(c), respectively. While ordered regions appear aligned near the boundaries, crystalline phases in the central regions are not aligned with the boundary. We simultaneously recorded a stack of

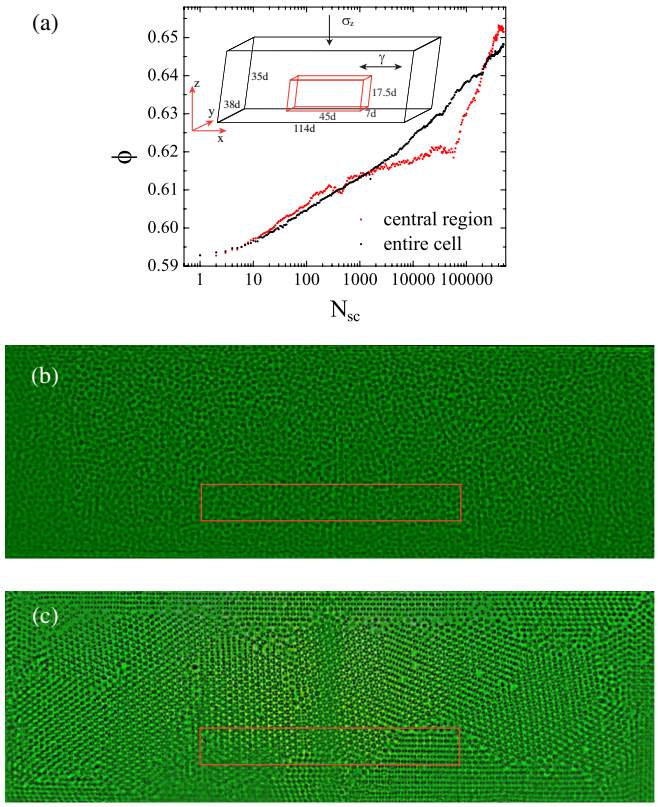

FIG. 1 (color online). (a) The volume fraction as a function of shear cycle number measured inside the viewing volume (red/gray) and in the entire cell (black). Inset: Schematic diagram of the shear cell and the central region selected for analysis. (b)–(c) Transversal view of the shear cell 10 mm from the top of the system: the initial packing, before applying shear deformations (b), and after 5×10^5 shear cycles (c).

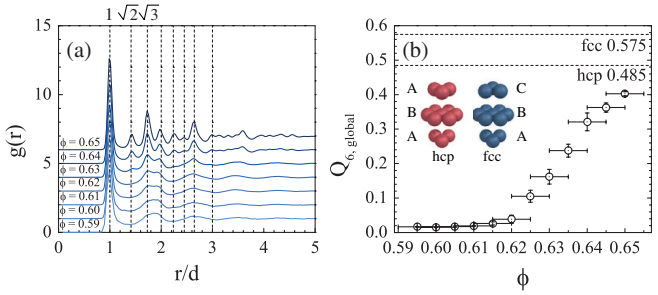

FIG. 2 (color online). (a) A curtain plot of the radial distribution function $g(r)$ as a function of normalized distance r/d for several volume fractions. Above $\phi = 0.63$, several peaks corresponding to a fcc or hcp lattice become visible. (b) Plot of $Q_{6,\mathrm{global}}$ versus ϕ. The sudden increase in the $Q_{6,\mathrm{global}}$ value indicates the beginning of the crystallization. Inset: The layers indicated by A, B, and C repeat with different periods for hcp and fcc symmetries.

images in a $44d \times 7d \times 17d$ volume in a central region of the cell $6d$ from the front wall and the bottom of the cell as indicated in Fig. 1(a) to avoid direct boundary effects. Figure 1 shows that ϕ obtained in this region follows, up to $N_{\mathrm{sc}} \sim 1000$ the overall trend except with larger fluctuations due to the smaller size of the observation window. For the next $N_{\mathrm{sc}} \sim 100\,000$, the volume fraction of the entire cell is systematically larger than in the central region. This difference could be explained by the fact that the boundary-induced crystallization starts to grow inside the packing. At $N_{\mathrm{sc}} \sim 100\,000$, a significant increase in the value of the packing volume fraction in the central region can be observed which coincides with the beginning of the crystal growth in bulk, as will be discussed later in the text. After half a million shear cycles, the packing volume fraction of the entire cell and in bulk converge to a similar value as the entire packing becomes a polycrystalline structure.

Figure 2(a) shows the radial density distribution function $g(r)$ as a function of distance r to characterize the development of spatial order with ϕ. In the case of a random system (liquid or amorphous solid), there is only short range order, and therefore only the nearest coordination shells are visible, while for a crystalline solid, $g(r)$ exhibit sharp peaks. Figure 2(a) shows that the system remains in a disordered state until $\phi \sim 0.62$, when a small shoulder in the second peak of $g(r)$ signals the appearance of ordered domains [14]. The bond orientation order parameter Q_6 is typically used to characterize the appearance of global hexagonal order and is obtained by using [15,16]

$$Q_l \equiv \left(\frac{4\pi}{(2l+1)} \sum_{m=-l}^{m=l} |\langle Y_{lm}(\Theta(\vec{r}), \Phi(\vec{r}))\rangle|^2 \right)^{1/2}, \quad (1)$$

with $l = 6$. Here, Y_{lm} are the spherical harmonics, $\Theta(\vec{r})$ is the polar angle, $\Phi(\vec{r})$ is the azimuthal angle, $\vec{r}$ is the vector between a particle and its pair, and the angled brackets indicate averaging over particle pairs. If averaging is performed over all pairs of particles in the system, then one obtains a measure of the global orientational order $Q_{l,\mathrm{global}}$ in the system, whereas, if the averaging is performed over nearest neighbors—defined as particles within the distance to the first minima in $g(r)$—then a local measure of orientational order $Q_{l,\mathrm{local}}$ is obtained. For disordered structures, Q_6 goes as the inverse of the number of particle pairs used in the average and is small [17]. But its value becomes significantly larger for ordered systems and reaches 0.575 for a fcc crystal [17]. In Fig. 2(b), we plot global $Q_{6,\mathrm{global}}$ as a function of ϕ averaged over a small 0.05 interval of ϕ to reduce noise. The value of $Q_{6,\mathrm{global}}$ is close to zero for packing fractions less than $\phi = 0.62$ but is then observed to increase sharply consistent with the onset of crystallization. Both these global measures show that an ordering transition indeed occurs in our granular system around the random close packing fraction ϕ_{rcp}.

To identify the development of crystallites and their symmetry, we calculate the local bond orientation order metric $Q_{4,\mathrm{local}}$ and $Q_{6,\mathrm{local}}$ for each particle in the observation window. Making a scatter plot of these two measures

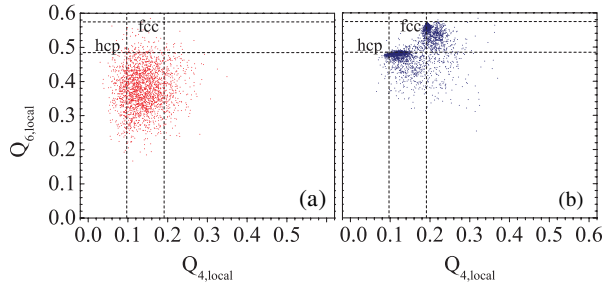

FIG. 3 (color online). Scatter plot of $Q_{4,\mathrm{local}}$ versus $Q_{6,\mathrm{local}}$ for the packing (a) before shear is applied, $\phi = 0.59$, and (b) $N_{\mathrm{sc}} = 5 \times 10^5$, $\phi = 0.65$. Each point corresponds to a particular particle. At $\phi = 0.65$, most of the points are located near hcp and fcc regions.

helps us distinguish clearly if hexagonal close packed (hcp) or face centered cubic (fcc) symmetry are present [see the inset in Fig. 2(b)]. Figure 3 shows that the points are broadly distributed before application of shear but clearly cluster around the values expected for fcc and hcp structure for $N_{\mathrm{sc}} = 5 \times 10^5$. The lack of any other peaks also implies that no other type of crystalline order develops in our system. In subsequent analysis, we choose a narrow range $0.08 \leq Q_{4,\mathrm{local}} \leq 0.16$, $0.46 \leq Q_{6,\mathrm{local}} \leq 0.5$ to label hcp and $Q_{4,\mathrm{local}} \geq 0.175$, $Q_{6,\mathrm{local}} \geq 0.54$ to label fcc regions.

Figure 4 shows particles in the midplane of the packings with different shades depending on whether they belong to fcc or hcp configuration. (The entire sequence is shown as a movie in the Supplemental Material [12].) It can be noted that, even for $\phi < \phi_{\mathrm{rcp}}$, small hcp clusters are distributed inside the system. These ordered clusters were initially observed to appear and disappear quite frequently but become more stable with increasing ϕ. By following the crystallites from one shear cycle to the next, we determined the probabilities p_g and p_s with which the crystallites grow or shrink [3]. Because these two probabilities are equal at the critical size, we plot in Fig. 5(a) the difference between p_g and p_s as a function of the number of particles in the crystallite. From this plot we estimated the critical size of

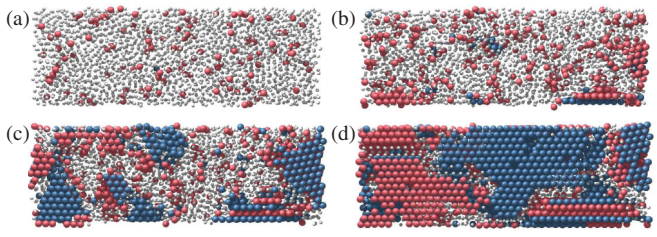

FIG. 4 (color online). A series of snapshots of the crystallization process; the red/dark gray spheres and the blue/light gray ones represent the particles with hcp and fcc symmetry, respectively. The particles in a random configuration are represented with a reduced size for clarity. (a) $N_{\mathrm{sc}} = 1$, $\phi = 0.59$; (b) $N_{\mathrm{sc}} = 5 \times 10^4$, $\phi = 0.62$; (c) $N_{\mathrm{sc}} = 1.5 \times 10^5$, $\phi = 0.64$; and (d) $N_{\mathrm{sc}} = 5 \times 10^5$, $\phi = 0.65$.

nuclei to be 10–60 particles. Remarkably, our results are similar to experimental studies of thermal colloidal suspensions [3], even though that study was conducted at constant volume with thermal frictionless hard spheres.

To test if shear has influence on the shape and orientation of the nucleating clusters, we calculate the moment of inertia tensor associated with each cluster of size $5 \leq N \leq 50$:

$$I_{jk} = \sum_{i=1}^{N} (r_i^2 - x_{i,j} x_{i,k}), \tag{2}$$

where N is the number of particles in a cluster, i labels the particles, and j and k label the components of $\vec{r}$, the vector from particle i to the cluster's center of mass. The square roots of the eigenvalues of the moment of inertia tensor denoted by $\lambda_{1,2,3}$ are shown in Fig. 5(b). For a spherical nucleus, these values should be identical. Because the principal radii of the ellipsoid fitting the cluster are inversely proportional to $\lambda_{1,2,3}$, we find that the average shape of the nuclei is nonspherical, with the principal radii being roughly in a 2:1:1 ratio [see Fig. 5(b)]. The eigenvectors of the moment of inertia tensor then allow us to determine the orientation of the nuclei. We plot the histogram of the polar angle θ from the positive z axis (shear gradient direction) and the azimuthal angle ϕ in the xy

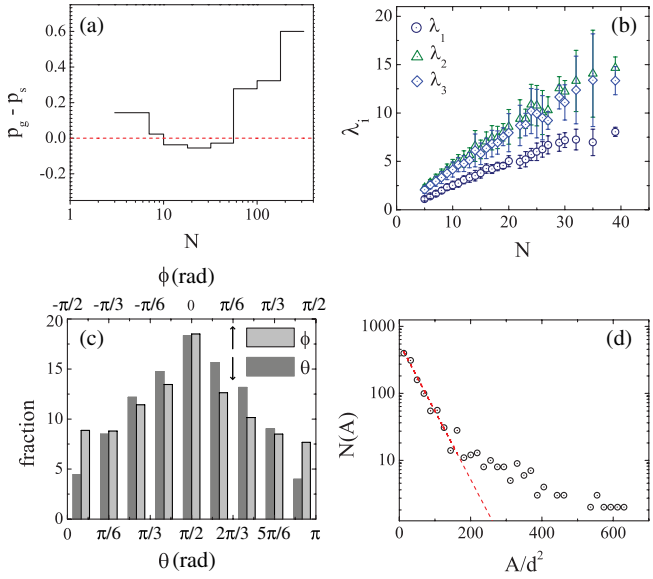

FIG. 5 (color online). (a) The difference between the probabilities of a crystalline nucleus to grow and shrink as a function of the number of particles in the crystallite. When these two probabilities become equal, the nucleus reaches a critical size. (b) Square root of the eigenvalues of the moments of inertia tensor as a function of the number of particles in the nucleus. (c) The histogram of the polar angle and the azimuthal angle made by the longest axis of the ellipsoid associated to each cluster. (d) The number of nuclei $N(A)$ as a function of the nucleus surface area, approximated by the area of a prolate spheroid. The line represents an exponential fit to the initial decay.

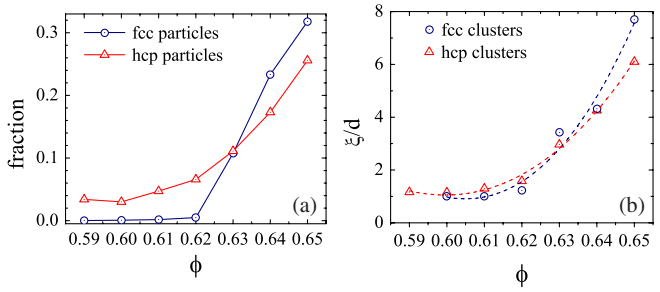

FIG. 6 (color online). (a) The fraction of each crystalline species as a function of the packing volume fraction. (b) Correlation length ξ of crystalline clusters normalized by the particle diameter. The dashed curves are drawn as a guide to the eye.

plane from the x axis (shear direction), made by the longest axis of the ellipsoid, in Fig. 5(c), respectively. The peaks are observed at $\theta = \pi/2$ and $\phi = 0$, showing that the orientation of the long axis of the clusters is predominantly aligned with the shear axis.

In classical nucleation theory [18], free energy of an ordered nucleus that emerges from a disordered liquid contains two terms: the bulk term, which is negative and proportional to the volume of the nucleus, and the surface term, which is proportional with the liquid-solid surface free energy γ and the area of the interface A. For small nuclei ($N \ll N_c$), the surface term dominates and the number of the crystallites is expected to be $N(A) \propto \exp[-\gamma' A/d^2]$ [3], where γ' is a dimensionless term corresponding to the surface free energy. We calculate the surface area of a crystallite as the area of the ellipsoid associated with it and plot the corresponding histogram in Fig. 5(d). From the exponential fit to the initial decay, we determine $\gamma' \simeq 0.023 \pm 0.002$. Both the overall decay and the scale of the decay is consistent with that obtained in experiments with thermal colloids [3], but it is difficult to extend this analogy further to calculate the surface tension because temperature is not well defined in granular systems.

Next, we turn to how the crystallites grow beyond the nucleation phase, where some nuclei which reached the critical size start to grow, while new critical nuclei continue to be formed. Above $\phi \simeq 0.64$, all nuclei reached the critical size, and the growing process becomes more accelerated, with the growth of large clusters at the expense of the smaller ones [Figs. 4(c) and 4(d)]. In Fig. 6(a), we show the fraction of each crystalline species observed in our experiments as a function of ϕ. We observe that, once the crystal starts to grow above $\phi \sim 0.62$, the number of fcc-like particles jumps, with a greater fraction at the highest volume fraction reached in our experiments. Recent studies with colloidal hard spheres have reported a random stacking in the crystal nuclei [3,19]. However, in slowly grown colloidal crystals, a clear tendency towards fcc order has been seen [20]. These results can be explained by the fact that, for hard sphere systems, the free energy difference between hcp and fcc order is very small and the equilibration time is very long [21–23]. In order to have an estimate of the scale of the crystal domains in our experiments, we calculate the correlation length corresponding to the size of the observed domains of fcc and hcp phases [24]:

$$\xi = \frac{2\sum_s R_g^2(s) s^2 n_s}{\sum_s s^2 n_s}. \quad (3)$$

Here n_s is the number of clusters of size s, and $R_g(s)$ is their radius of gyration. Figure 6(b) shows that the correlation length of the fcc clusters increases more rapidly than the correlation length of the hcp clusters above ϕ_{rcp}. Thus, we conclude that the two phases, fcc and hcp, are well separated in our system and distinct from a random hexagonal close packed phase, in addition to the observation that the fcc phase becomes more abundant. A similar evolution has also been observed in numerical simulations with hard spheres as well [25].

In summary, we have shown with delicate experiments that sheared granular systems undergo homogeneous nucleation in addition to inhomogeneous nucleation at sidewalls. We measured the size and the symmetry of the ordered phases in athermal frictional hard sphere systems for the first time and showed the influence of shear on the shape and orientation of the crystallites. The process of nucleation is also surprisingly similar to the one observed in computer simulations [19] and experiments [3] on thermal colloidal hard sphere suspensions, suggesting that the development of crystallization in hard sphere systems is far more universal than previously anticipated.

We thank V. Kumaran and H. Gould for stimulating discussions. This work was supported by the National Science Foundation under NSF Grant No. CBET-0853943.

[1] M. D. Haw, W. C. K. Poon, and P. N. Pusey, Phys. Rev. E **57**, 6859 (1998).
[2] U. Gasser, J. Phys. Condens. Matter **21**, 203101 (2009).
[3] U. Gasser, E. R. Weeks, A. Schofield, P. N. Pusey, and D. A. Weitz, Science **292**, 258 (2001).
[4] M. Hecke, J. Phys. Condens. Matter **22**, 033101 (2010).
[5] L. E. Silbert, D. Ertaş, G. S. Grest, T. C. Halsey, and D. Levine, Phys. Rev. E **65**, 031304 (2002).
[6] V. Kumaran, J. Fluid Mech. **632**, 109 (2009).
[7] M. Nicolas, P. Duru, and O. Pouliquen, Eur. Phys. J. E **3**, 309 (2000).
[8] J.-C. Tsai, G. A. Voth, and J. P. Gollub, Phys. Rev. Lett. **91**, 064301 (2003).
[9] S. Slotterback, M. Toiya, L. Goff, J. F. Douglas, and W. Losert, Phys. Rev. Lett. **101**, 258001 (2008).
[10] A. Panaitescu and A. Kudrolli, Phys. Rev. E **81**, 060301 (2010).

[11] The liquids have a density of 1.0×10^3 k gm^{-3} and viscosity of 2.2×10^{-2} Pa s and were obtained from Cargille Laboratories.
[12] See Supplemental Material at http://link.aps.org/supplemental/10.1103/PhysRevLett.108.108001 for a movie of the development of the crystallization in a slice inside the granular packing located 10d from the front wall (M1) and a 3D reconstruction of the same region (M2) after particle tracking.
[13] G. Scott and D. M. Kilgour, J. Phys. D **2**, 863 (1969).
[14] T. M. Truskett, S. Torquato, S. Sastry, P. G. Debenedetti, and F. H. Stillinger, Phys. Rev. E **58**, 3083 (1998).
[15] P. J. Steinhardt, D. R. Nelson, and M. Ronchetti, Phys. Rev. B **28**, 784 (1983).
[16] A. R. Kansal, S. Torquato, and F. H. Stillinger, Phys. Rev. E **66**, 041109 (2002).
[17] M. Rintoul and S. Torquato, J. Chem. Phys. **105**, 9258 (1996).
[18] P. G. Debenedetti, *Metastable Liquids* (Princeton University, Princeton, NJ, 1996).
[19] T. Kawasaki and H. Tanaka, Proc. Natl. Acad. Sci. U.S.A. **107**, 14 036 (2010).
[20] P. N. Pusey, W. van Megen, P. Bartlett, B. J. Ackerson, J. G. Rarity, and S. M. Underwood, Phys. Rev. Lett. **63**, 2753 (1989).
[21] L. V. Woodcock, Nature (London) **385**, 141 (1997).
[22] S.-C. Mau and D. A. Huse, Phys. Rev. E **59**, 4396 (1999).
[23] Z. Cheng, P. M. Chaikin, J. Zhu, W. B. Russel, and W. V. Meyer, Phys. Rev. Lett. **88**, 015501 (2001).
[24] Y. Jin and H. A. Makse, Physica (Amsterdam) **389A**, 5362 (2010).
[25] V. Luchnikov, A. Gervois, P. Richard, L. Oger, and J. P. Troadec, J. Mol. Liq. **96–97**, 185 (2002).